Journal of Materials Chemistry A

Accepted Manuscript

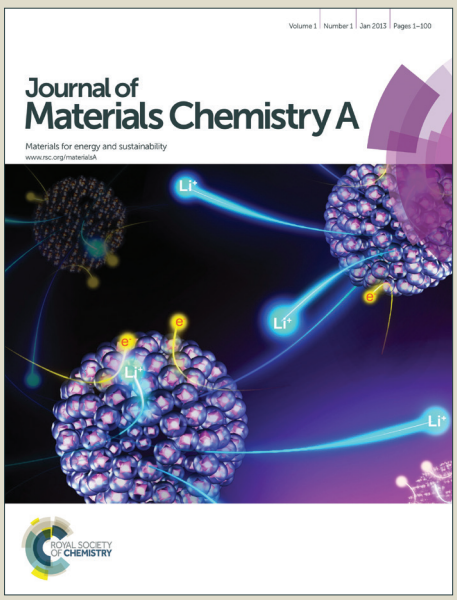

ROYAL SOCIETY OF CHEMISTRY

www.rsc.org/materialsA

Journal of Materials Chemistry A RSCPublishing

COMMUNICATION

Iron Oxide Nanostructures as Highly Efficient Heterogeneous Catalyst for Mesoscopic Photovoltaics

Cite this: DOI: 10.1039/xoxxoooooox

Liang Wang,[a] Yantao Shi,*[a] Hong Zhang,[a] Xiaogong Bai,[a] Yanxiang Wang[c] and Tingli Ma*[ab]

Received ooth January 2012,
Accepted ooth January 2012

DOI: 10.1039/xoxxoooooox

www.rsc.org/

The Fe_3O_4 with hierarchical structures was successfully synthesized and introduced into dye-sensitized solar cells as counter electrode. The power conversion efficiency of 7.65 % based on Fe_3O_4 was completed, superior to the value of pyrolytic Pt (6.88 %) and close to that for sputtered Pt (7.87 %).

Dye-sensitized solar cells (DSCs), as a promising candidate for traditional counterparts, have attracted widespread attentions due to their superior features, such as high efficiencies, simple and environmental friendly fabrication procedures, as well as flexible design in colors and patterns.[1] In the past two decades, power conversion efficiencies (PCEs) of 13.0% has been achieved in 2014, enabling them more feasible for practical applications.[2] A typical DSC is usually composed of dye-sensitized photoanode, electrolyte with redox couple (i. e., I_3^-/I^-) and counter electrode (CE), which actually serves as catalyst for reduction I_3^- to I^-.[1] CE materials with high electrocatalytic activity and abundant sources are desired in terms of achieving high efficiency and reducing the cost of DSCs. Traditional Pt is a highly efficient catalytic material for use as CE in DSCs. But Pt is a kind of noble metal, scarce and unfavorable to large-scale fabrications of DSCs in future. As a matter of fact, in recent years some carbons, functional polymers, and even inorganic materials have been proved also efficient as CE candidates in DSCs.[3-21] Whereas, there are still some deficiencies that need to be improved for further perfecting DSCs, such as the production cost is still high, part of the preparation procedures are complicated and hinder the large-area application, some is not easy to be repeated, the stability is not so well, and so on. Therefore, developing new CE catalysis withlow cost, simple procedure and high electrocatalytic activity are highly desired.

Ferrum (Fe) is a transition metal that ranks the fourth among the most abundant elements on the earth. Meanwhile, various iron compounds can be formed based on different compositions, valence states and crystal phases. In recent years, nanostructures of iron compounds like oxides, carbides and sulfides have been widely developed for catalysis,[22, 23] electrodes of secondary batteries,[24-27] waste water treatment[28, 29] and targeted agents in biomedicine.[30] Additionally, in the field of DSCs FeS_2[31], rosin carbon/Fe_3O_4[32] and graphitic carbon/Fe_3C[33] had been used as CE catalysts and exhibited good performances. Recently, via first-principle quantum chemical calculations, Yang and co-workers theoretically predicted and experimentally proved that α-Fe_2O_3 was a superior catalyst for fabrication of CE in DSCs.[34] As all know, Fe_3O_4 is an important iron compound, which is also a conductor. Unit cell of Fe_3O_4 is composed of 32 oxygen and 24 Fe atoms, among which 1/3 are in the form of Fe^{3+} and occupy 8 (of 64) tetrahedron, whereas 2/3 occupy 16 (of 32) octahedron with equal numbers of Fe^{2+} and Fe^{3+}. Therefore, electrons can be transferred through hopping along the octahedral iron chains.[35] Until now, few studies were published on applications of different valence state materials in DSCs.

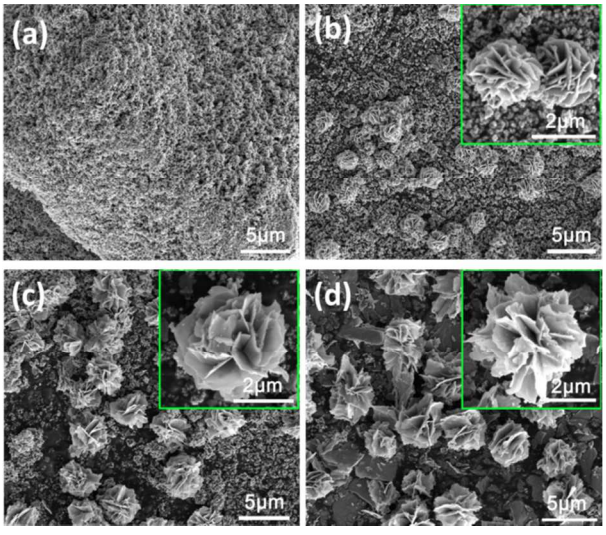

Figure 1. The SEM images of flower-like Fe_3O_4 forming process at different reaction temperatures (a): 165 ℃, (b): 175 ℃, (c): 185 ℃ and (d): 195 ℃.

Herein, Fe_3O_4 micron flowers composed of nanosheets were prepared by a hydrothermal route. By controlled annealing Fe_3O_4 at different conditions, α-Fe_2O_3 and γ-Fe_2O_3 were respectively obtained via phase transformation, but the original morphology of hierarchical structure was almost unaffected. These three iron oxides were applied as CEs for DSCs. Result showed that, compared with α-Fe_2O_3, both Fe_3O_4 and γ-Fe_2O_3 were more superior in terms of electro-catalytic activity and photovoltaic performance in DSCs. Moreover, by optimizing the nanostructure of Fe_3O_4, further photovoltaic improvements were realized.

In order to clarify the formation process of flower-like Fe_3O_4, we extracted the products at different reaction stages, as shown in Figure 1. Figure 1(a) shows that, at the early stage (165 ^oC), in the product there are only nano-sized Fe_3O_4 particles. With increasing synthetic temperature to 175^oC, a few micron-sized hierarchical flowers can be observed (Figure 1(b)). At the third selected point (when temperature was 185^oC), hierarchical flowers turn into the dominant structures and in the meantime their sizes are further increased, as shown in Figure 1(c). Finally, for the one extracted at 195^oC, no nanoparticles are remained and the sample is entirely composed of the flower-like Fe_3O_4 (Figure 1(d)). It can be said that, external energy is crucial for oriented aggregation, by which these two dimensional nanosheets on the hierarchical Fe_3O_4 flower are formed. Phase transformation from Fe_3O_4 to α-Fe_2O_3 or γ-Fe_2O_3 was achieved by control of the sintered temperature and atmosphere, as shown in the supporting information. Using this strategy, we hardly found any morphology change (See Figure S1). The relevant XRD patterns and detailed peak assignments are summarized in the Figure 2.

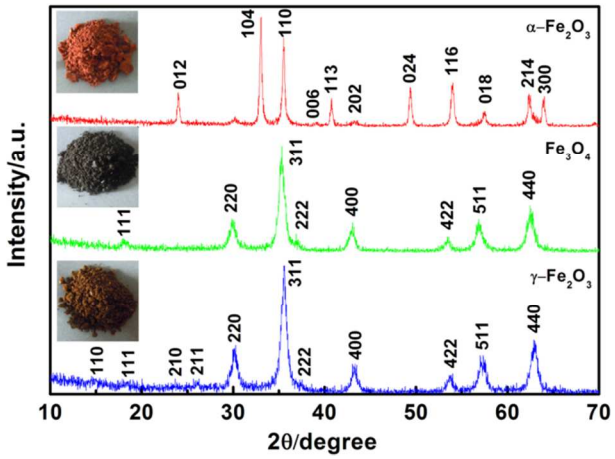

Figure 2. XRD patterns of the α-Fe_2O_3, Fe_3O_4, and γ-Fe_2O_3

Figure 3(a) shows *J-V* curves under 1 sun (AM 1.5G, 100mW cm^{-2}) illumination for the DSCs using five kinds of CEs, α-Fe_2O_3,Fe_3O_4,γ-Fe_2O_3 and two widely used references, pyrolytic Pt and sputtered Pt. The values of open-circuit photovoltage (V_{oc}), summarized in Table 1. With comparable J_{sc} and V_{oc}, however, short-circuit photocurrent density (J_{sc}), fill factor (*FF*) and PCEs are DSCs based on α-Fe_2O_3 gave relative low *FF* thus the PCE was only 5.59%, the worst one among these DSCs devices. By contrast, DSCs based on γ-Fe_2O_3 and Fe_3O_4 both exhibited improved *FFs* and PCEs. As CEs for DSCs, it was increased by the order from α-Fe_2O_3, γ-Fe_2O_3 to Fe_3O_4 in terms of photovoltaic performances. Our findings in this work suggested that γ-Fe_2O_3 and Fe_3O_4 were superior to α-Fe_2O_3 that has been proved a good candidate material for CE of DSCs. The PCE of 6.80% for Fe_3O_4-based was close to that based on pyrolytic Pt, but still lower than that of 7.93% for the one based on sputtered Pt. On the other hand, inherent mechanism affecting performances of DSCs should be revealed in detail.

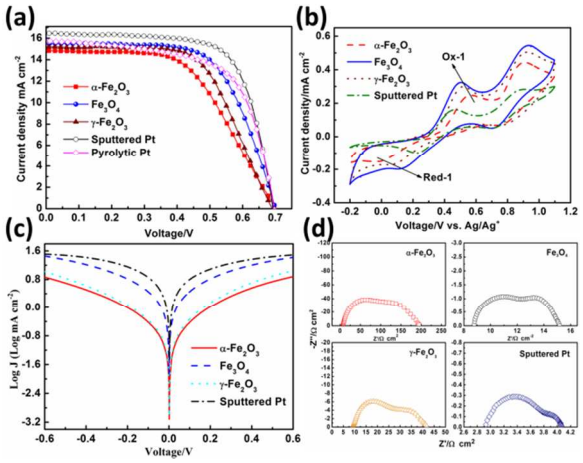

Figure 3. (a) Photocurrent density-voltage (*J-V*) of the DSCs using α-Fe_2O_3, Fe_3O_4, γ-Fe_2O_3, pyrolytic Pt and sputtered Pt CEs. (b) Cyclic voltammograms based on the four CEs in three electrodes system. (c) Tafel curves of different dummy cells that are CE/electrolyte/CE. (d) Nyquist plots based on different dummy cells that are similar to those used for the Tafel measurements.

Cyclic voltammetry (CV), Tafel polarization curves and electrochemical impedance spectra (EIS) were carried out to systematically reveal the relationship between catalytic activity and different iron oxides. Figure 3(b) shows the four CV curves based on three iron oxide CEs and sputtered Pt, respectively. Two pairs of redox peaks are observed in all of the curves. The redox peak can be assigned to the followed two reactions: $I_3^-+2e^- \leftrightharpoons 3I^-$ (lower potential peaks), $3I_2+2e^- \leftrightharpoons 2I_3^-$ (higher potential peaks). According to the former reaction, the CV plots show a cathodic reduction peak (Red-1) and an anodic oxide peak (Ox-1), corresponding to the reduction of I_3^- and oxidation of I^-, respectively. Under the working condition of DSCs, the CE is mainly responsible for catalyzing the reduction of I_3^- to I^-. Therefore, the left redox peak is the key object of study for understanding the electrocatalytic activity. As shown in Figure 3(b), the peak-to-peak separations (E_{pp}) are 0.572 V, 0.452 V and 0.372 V for α-Fe_2O_3, γ-Fe_2O_3 and Fe_3O_4, respectively. Smaller E_{pp}, together

Table 1. Photovoltaic parameters of the DSCs using α-Fe_2O_3, Fe_3O_4, γ-Fe_2O_3pyrolytic Pt and sputtered Pt CEs and EIS parameters of symmetrical cells using α-Fe_2O_3, Fe_3O_4, γ -Fe_2O_3 and sputtered Pt electrodes

Samples	*V*oc/V	*J*sc/mA cm^{-2}	*FF*	*Eff.*/%	*R*s/Ω cm^2	R_{ct}/Ω cm^2	Z_N/Ω cm^2
α-Fe_2O_3	0.698±0.005	14.63±0.15	0.53±0.01	5.59±0.16	7.29	99.71	95.63
Fe_3O_4	0.701±0.003	15.41±0.17	0.63±0.01	6.80±0.21	8.75	4.30	4.28
γ-Fe_2O_3	0.690±0.004	15.0±0.31	0.61±0.01	6.39±0.13	9.07	17.74	14.15
Sputtered Pt	0.695±0.005	16.13±0.27	0.70±0.01	7.93±0.15	2.97	1.77	0.64
Pyrolytic Pt	0.694±0.003	15.79±0.21	0.63±0.01	6.89±0.25	-	-	-

with its higher cathodic peak current density, both indicate that Fe_3O_4 as electrocatalyst is more efficient than others iron oxides in this experiment.[8] Figure 3(c) demonstrates the Tafel polarization curves of the symmetrical cells. The cell based on Fe_3O_4 shows clearly larger slope than the other iron oxides, indicating a higher exchange current density (J_0) and limiting current density (J_{lim}). The results also confirm that the highest electrocatalytic activity has been achieved by Fe_3O_4 CE among these three iron oxides. The Nyquist curves based on above symmetrical cells was shown in Figure 3(d) and Table 1. Typically, there are two semicircles, which are defined as charge-transfer resistance (R_{ct}) at the CE/electrolyte interface (left semicircle) and Nernst diffusion impedance (Z_N) of the redox couple in the electrolyte (right semicircle). The high frequency intercept on the real axis shows the series resistance (R_s). The R_{ct} value for the Fe_3O_4 CE is 4.30 Ω, which is much lower than that of α-Fe_2O_3 CE (99.71 Ω) and γ-Fe_2O_3 CE (17.74 Ω), and close to sputtered Pt (1.77 Ω). It means that Fe_3O_4 CE is more active than the other iron oxides for reducing of I_3^-. The Z_N is usually related with the diffusion rate of the redox couple in electrolyte. Generally, diffusion rate of ion is highly connected with the physical structure of materials without regarding to the interaction. However, in CE/electrolyte interface, the main role of CE is accelerating catalytic reduction of I_3^-. Due to different catalytic activity of the three iron oxides, just as shown in the CV and Tafel parts, different I^- concentration will be generated. In other words, the higher catalytic activity accompanies with higher concentration of I^-, further higher diffusion driving force, which results in the different diffusion resistances of α-Fe_2O_3, γ -Fe_2O_3, and Fe_3O_4 CEs. Therefore, different catalytic activity should be responsible for different Z_N under similar physical structure. For I_3^- on Fe_3O_4 CE, the value is 4.28 Ω, much smaller than those for α-Fe_2O_3 CE (95.63 Ω) and γ-Fe_2O_3 CE (14.15Ω) under the same test conditions. Apparently, the improved PCE should be attributed to the decrease of both R_{ct} and Z_N as Fe_3O_4 CE was employed.

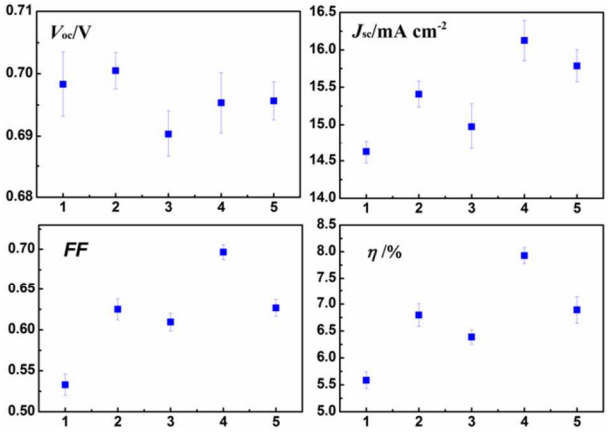

Figure 4. Photovoltaic parameters (V_{oc}, J_{sc}, *FF* and η) extracted from *J-V* measurements of a series of DSCs with different CEs; 1. α-Fe_2O_3, 2. Fe_3O_4, 3. γ-Fe_2O_3, 4. Sputtered Pt and 5. Pyrolytic Pt.

Figure 4 shows the photovoltaic parameters derived from *J-V* measurements of a series of DSCs based on different CEs. It is clearly that all parameters of DSCs constructed with different CEs show good repeatability during the same conditions. The error bar has also been shown in Table 1 and Table 2 for religious comparison. The relevant statistical analysis was also performed and shown in ESI.

As we all know, the more active sites the catalyst has, the more active it will become. In this work, we optimized the nanostructure of Fe_3O_4 flower. Figure 5shows the *J-V* curves of DSCs based on Fe_3O_4 CE with different concentration of reactants, where the concentration were decreased to 1/2 (Fe_3O_4-0.5) and 1/10 (Fe_3O_4-0.1) of the original concentration value (Figure 1 (D)), respectively. The SEM image of Fe_3O_4-0.1 is also shown in Figure 4 as an illustration. Along with the decrease of concentration, we successfully enhanced the nanosheets packing density and the homogeneity of Fe_3O_4 hierarchical flowers. Thus, within a given volume or thickness, our improved Fe_3O_4 flowers can offer more reaction sites. The detailed *J-V* parameters are summarized in Table 2. It is clearly that Fe_3O_4-0.1-based DSCs demonstrates the notable PCE of 7.65%, much higher than the values of Fe_3O_4 and Fe_3O_4-0.5, superior to the value of pyrolytic Pt (6.88 %) and close to that of the sputtered Pt (7.87 %). For religious comparison，the statistical analysis on comparisions of PCEs for solar cells were also conducted (ESI, the last part)，which give the further proof on our conclusions about the photovoltaic performance of developed Fe_3O_4 and Pt CEs.[36] The corresponding electrochemical measurements have also been employed and shown in the ESI (Figure S3, S4 and S5). Finally, the stability of Fe_3O_4 CE was tested in I_3^-/I^- system by CV measurement. There was no clearly declined current density and peak shift after 100 cycles, which showed the good stability of the developed Fe_3O_4 CE.[10] (Figure S6)

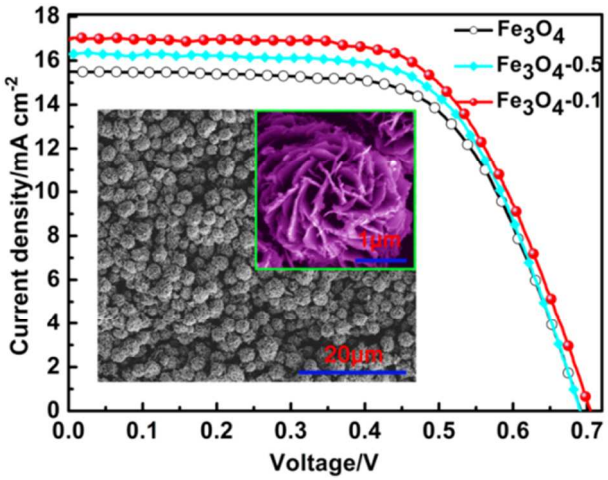

Figure 5. *J-V* curves of the DSCs using Flower-like Fe_3O_4 CEs by different concentration of reactants, where the concentration were decreased to 1/2 and 1/10 of the original concentration value (Figure 1 (D)), respectively. The inset shows the SEM image of flower-like Fe_3O_4 with 1/10 concentration of reactants.

Table 2.Photovoltaic parameters of the DSCs usingFe_3O_4 CE prepared with different concentration of reactants.

Sample	V_{oc} /V	J_{sc} /mA cm^{-2}	*FF* /%	η. /%
Fe_3O_4	0.681±0.007	15.18±0.21	0.63±0.01	6.76±0.11
Fe_3O_4-0.5	0.683±0.006	15.96±0.35	0.64±0.01	7.17±0.14
Fe_3O_4-0.1	0.693±0.008	16.67±0.28	0.63±0.01	7.65±0.12
Sputtered Pt	0.679±0.005	16.29±0.19	0.69±0.02	7.87±0.14
Pyrolytic Pt	0.682±0.006	16.08±0.24	0.60±0.17	6.88±0.12

Conclusions

In conclusion, the heterogeneous flower-like α-Fe_2O_3, Fe_3O_4 and γ-Fe_2O_3 hierarchical structures were successfully synthesized and introduced into DSCs as CEs. The results of electrochemical measurement showed that Fe_3O_4 exhibited excellent performance when compared with the other two iron oxides. After structural optimization by enhancing the packing density of the nanosheets, more reaction sites were offered by

per Fe_3O_4 flower. Finally, DSCs based on Fe_3O_4 CE achieved notable power conversion efficiency, superior to the value of pyrolytic Pt and close to that for sputtered Pt. Our findings in this work suggested that the Fe_3O_4 could be used as a good candidate CE material for DSCs.

This work is supported by National Natural Science Foundation of China (Grant No. 51273032, 91333104), International Science & Technology Cooperation Program of China (Grant No. 2013DFA51000) and the Fundamental Research Funds for the Central Universities (Grant No. DUT12RC(3)57). This research was also supported by the State Key Laboratory of Fine Chemicals of China.

Notes and references

[a] State Key Laboratory of Fine Chemicals, College of Chemistry, Dalian University of Technology (DUT) 2 Linggong Rd., 116024, Dalian, China E-mail: tinglima@dlut.edu.cn and shiyantao@dlut.edu.cn

[b] Graduate School of Life Science and Systems Engineering Kyushu Institute of Technolog 2-4 Hibikino, Wakamatsu, Kitakyushu, Fukuoka, 808-0196, Japan

[c] School of Material Science and Engineering, JingDeZhen Ceramic Institute, JingDeZhen, China.

1.B. O'regan and M. Grätzel, *nature*, 1991, **353**, 737.

2.S. Mathew., A. Yella, P. Gao, R. Humphry-Baker, B. F. E. Curchod,N. Ashari-Astani, I. Tavernelli, U. Rothlisberger, M. K. Nazeeruddinand M. Grätzel, *Nat. Chem.*, 2014, **6**, 242.

3.X. Xin, M. He, W. Han, J. Jung and Z. Lin, *Angew. Chem. Int. Ed.*, 2011, **50**, 11739.

4.X. Zheng, J. Guo, Y. Shi, F. Xiong, W.-H. Zhang, T. Ma and C. Li, *Chem. Commun.*, 2013, **49**, 9645.

5.J.Y. Lin, C.-Y. Chan and S.-W. Chou, *Chem. Commun.*, 2013, **49**, 1440.

6.F. Gong, H. Wang, X. Xu, G. Zhou and Z.S. Wang, *J. Am. Chem. Soc.*, 2012, **134**, 10953.

7.T. N. Murakami, S. Ito, Q. Wang, M. K. Nazeeruddin, T. Bessho, I. Cesar, P. Liska, R. Humphry-Baker, P. Comte and P. Péchy, *J. Electrochem. Soc.*, 2006, **153**, A2255.

8.Z. Wang, F. Gong, X. Xu, Z. Li and G. Zhou, *Chem. Commun.*, 2013, **49**, 1437.

9.M. Wang, A. M. Anghel, B. Marsan, N. L. Cevey Ha, N. Pootrakulchote, S. M. Zakeeruddin and M. Grätzel, *J. Am. Chem. Soc.*, 2009, **131**, 15976.

10.J. D. Roy-Mayhew, D. J. Bozym, C. Punckt and I. A. Aksay, *ACS nano*, 2010, **4**, 6203.

11.X. Zhang, X. Chen, K. Zhang, S. Pang, X. Zhou, H. Xu, S. Dong, P. Han, Z. Zhang, C. Zhang and G. Cui, *J. Mater. Chem. A*, 2013, **1**, 3340.

12.L. Cheng, Y. Hou, B. Zhang, S. Yang, J. Guo, L. Wu and H. Yang, *Chem. Commun.*, 2013, **49**, 5945.

13.H. Zhou, Y. Shi, Q. Dong, Y. Wang, C. Zhu, L. Wang, N. Wang, Y. Wei, S. Tao and T. Ma, *J. Mater. Chem. A*, 2014, **2**, 4347.

14.M. Wu, Y. Wang, X. Lin, N. Yu, L. Wang, L. Wang, A. Hagfeldt and T. Ma, *Phys. Chem. Chem. Phys.*, 2011, **13**, 19298.

15.W. Zhao, T. Lin, S. Sun, H. Bi, P. Chen, D. Wan and F. Huang, *J. Mater. Chem. A*, 2013, **1**, 194.

16.M. Wu, X. Lin, Y. Wang, L. Wang, W. Guo, D. Qi, X. Peng, A. Hagfeldt, M. Grätzel and T. Ma, *J. Am. Chem. Soc.*, 2012, **134**, 3419.

17.M. Wu, X. Lin, T. Wang, J. Qiu and T. Ma, *Energy Environ. Sci.*, 2011, **4**, 2308.

18.T.L. Zhang, H.-Y. Chen, C.Y. Su and D.-B. Kuang, *J. Mater. Chem. A*, 2013, **1**, 1724.

19.Z. Wei, Y. Qiu, H. Chen, K. Yan, Z. Zhu, Q. Kuang and S. Yang, *J. Mater. Chem. A*, 2014, **2**, 5508.

20.H. Xu, C. Zhang, Z. Wang, S. Pang, X. Zhou, Z. Zhang and G. Cui, *J. Mater. Chem. A*, 2014, **2**, 4676.

21.J. Guo, Y. Shi, C. Zhu, L. Wang, N. Wang and T. Ma, *J. Mater. Chem. A*, 2013, **1**, 11874.

22.S.W. Cao and Y.J. Zhu, *J. Phys. Chem. C*, 2008, **112**, 6253.

23.A. A. Tahir, K. G. U. Wijayantha, S. Saremi-Yarahmadi, M. Mazhar and V. McKee, *Chem. Mater.*, 2009, **21**, 3763.

24.Y.G. Zhu, J. Xie, G. Cao, T. Zhu and X. Zhao, *RSC Adv.*, 2013, **3**, 6787.

25.R. Wang, C. Xu, J. Sun, L. Gao and C. Lin, *J. Mater. Chem. A*, 2013, **1**, 1794.

26.T. Yoon, C. Chae, Y.K. Sun, X. Zhao, H. H. Kung and J. K. Lee, *J. Mater. Chem.*, 2011, **21**, 17325.

27.Y. Deng, Q. Zhang, S. Tang, L. Zhang, S. Deng, Z. Shi and G. Chen, *Chem. Commun.*, 2011, **47**, 6828.

28.D. Zhang, C. Lu, Y. Ni, Z. Xu and W. Zhang, *CrystEngComm*, 2013, **15**, 4755.

29.L. S. Zhong, J. S. Hu, H. P. Liang, A. M. Cao, W. G. Song and L. J. Wan, *Adv. Mater.*, 2006, **18**, 2426.

30.P. Tartaj, M. P. Morales, T. Gonzalez-Carreño, S. Veintemillas-Verdaguer and C. J. Serna, *Adv. Mater.*, 2011, **23**, 5243.

31.Y.C. Wang, D.-Y. Wang, Y.-T. Jiang, H.-A. Chen, C.-C. Chen, K.-C. Ho, H.-L. Chou and C.-W. Chen, *Angew. Chem. Int. Ed.*, 2013, **52**, 6694.

32.L. Wang, Y. Shi, Y. Wang, H. Zhang, H. Zhou, Y. Wei, S. Tao and T. Ma, *Chem. Commun.*, 2014, **50**, 1701.

33.Y. Liao, K. Pan, L. Wang, Q.-J. Pan, W. Zhou, X. Miao, B. Jiang, C. Tian, G. Tian, G. Wang and H. Fu, *ACS Appl. Mater. Interfaces*, 2013, **5**, 3663.

34.Y. Hou, D. Wang, X. H. Yang, W. Q. Fang, B. Zhang, H. F. Wang, G. Z. Lu, P. Hu, H. J. Zhao and H. G. Yang, *Nat. Commun.*, 2013, **4**, 1.

35.T. Kendelewicz, S. Kaya, J. T. Newberg, H. Bluhm, N. Mulakaluri, W. Moritz, M. Scheffler, A. Nilsson, R. Pentcheva and G. E. Brown, *J.Phys.Chem. C*, 2013, **117**, 2719.

36.E. J. Luber and J. M. Buriak, *ACS nano*, 2013, **7**, 4708.

